



The role of topological defects on the mechanical properties of single-walled carbon nanotubes

Daniela A. Damasceno & Caetano R. Miranda

To cite this article: Daniela A. Damasceno & Caetano R. Miranda (2021): The role of topological defects on the mechanical properties of single-walled carbon nanotubes, Philosophical Magazine, DOI: [10.1080/14786435.2021.1988174](https://doi.org/10.1080/14786435.2021.1988174)

To link to this article: <https://doi.org/10.1080/14786435.2021.1988174>



View supplementary material [↗](#)



Published online: 11 Oct 2021.



Submit your article to this journal [↗](#)



Article views: 59



View related articles [↗](#)



View Crossmark data [↗](#)



The role of topological defects on the mechanical properties of single-walled carbon nanotubes

Daniela A. Damasceno  and Caetano R. Miranda 

Departamento de Física dos Materiais e Mecânica, Instituto de Física, Universidade de São Paulo (USP), São Paulo, Brasil

ABSTRACT

Carbon nanotubes (CNTs) are among the most employed nanomaterials in developing new technologies. Their applicability requires a fundamental understanding of the chirality and defect effects on the mechanical properties. In this study, molecular dynamics (MD) simulations were performed to investigate the mechanical response of defective single-walled carbon nanotubes (SWCNTs) under tension loading. The Stones-Wales, monovacancy, and the divacancy reconstructions (585, 555777, and 555567777) defects were considered. In addition, we investigated the influence of the adaptive intermolecular reactive bond order (AIREBO) potential cut-off radii on the defect formation energy of SWCNTs. Our results reveal that the tensile strength properties are notably dependent on the chirality and defect configurations at strains over 8%. Energetically favourable defects have a high impact on the mechanical response of SWCNTs. A combination of certain defects may lead the control on the fracture pattern of the SWCNTs, which can significantly contribute to the designing of innovative nanostructures with tailored properties.

ARTICLE HISTORY



Received 27 February 2021
Accepted 27 September 2021

KEYWORDS

Carbon nanotubes; defects; fracture pattern; molecular modelling; fracture strength

Introduction

Carbon nanotubes (CNTs) [1] with a controllable diameter size [2] combined with their fast mass transport [3] and outstanding mechanical and physical properties [4,5] emerges as a great promise for filtering devices [6], interconnect systems [7], among others. Several experimental measurements [5,8–10] have confirmed the CNTs' remarkable mechanical properties. Despite this, various mechanical experiments do not agree with each other, and a wide range of Young's modulus [5,11], tensile strength [5,11], and strain [5,9] values can be found in the literature. The source of the differences in the reported values

CONTACT Caetano R. Miranda  cmiranda@if.usp.br  Departamento de Física dos Materiais e Mecânica, Instituto de Física, Universidade de São Paulo (USP), Rua do Matão, Travessa R, Nr. 187, Cidade Universitária, São Paulo, SP 05508-090, Brasil

 Supplemental data for this article can be accessed <https://doi.org/10.1080/14786435.2021.1988174>.

© 2021 Informa UK Limited, trading as Taylor & Francis Group

for mechanical properties may be related to the nanotube chirality and the presence of defects [12].

Chirality has a strong effect on the mechanical response of single-walled carbon nanotubes (SWCNTs). Experimental [8] and computational modelling [13] approaches have confirmed this effect. However, it is still not clear the chirality effects on the tensile strength properties of defective SWCNTs under different loading conditions. Defects are another factor that has a significant impact on the mechanical properties of CNTs [14,15]. They are naturally formed during the CNTs synthesis, or they are introduced in a controlled manner using novel routes for the synthesis.

The introduction of defects is often desirable to enhance some physical properties of CNTs [16–18]. Although many groups have recently succeeded in performing experiments with carbon nanotubes, performing these experiments in a controlled manner is still challenging. For this reason, computational modelling are an essential tool for calculating the CNTs properties considering different chirality and defects, which are usually intricate features to be attained and controlled by experimental measurements.

The formation energies, electronic and thermal properties of defective CNTs have been extensively studied [19–22]. Other studies employed the tight-binding calculations [23], molecular dynamics (MD) simulations [13,24–29], molecular mechanics calculations [15,30–34], and the atomic-scale finite element method [35] to investigate the buckling behaviour and Young's modulus of pristine CNTs. However, less attention has been paid to the effects of single and multiple topological defects on the mechanical response of SWCNTs [14,26,33], especially those with low formation energies.

This study presents a comprehensive fully atomistic modelling to investigate the effects of chirality and single and multiple defects on SWCNTs' mechanical response. MD calculations were carried out based on the adaptive intermolecular reactive bond order (AIREBO) potential [36]. We considered five types of defects, where their shape and orientation are based on experimental observations and ab-initio studies. In addition, it was discussed the influence of the AIREBO cut-off radii on the defect formation energy of SWCNTs. This contribution is timely as the effects of different radii on the formation energies have not been addressed in the literature.

Model and method

SWCNTs and topological defects

Figure 1 presents a schematic model of SWCNTs. The bond length of two carbon atoms is 1.42 Å [37]. The parameters n and m determine the chirality and diameter (ϕ) of the nanotubes. The directions zigzag (zz) with $n = 0$ and $m = 17$, chiral (*ch*) with $n = 9$ and $m = 11$, and armchair (*ar*) with $n = m = 10$

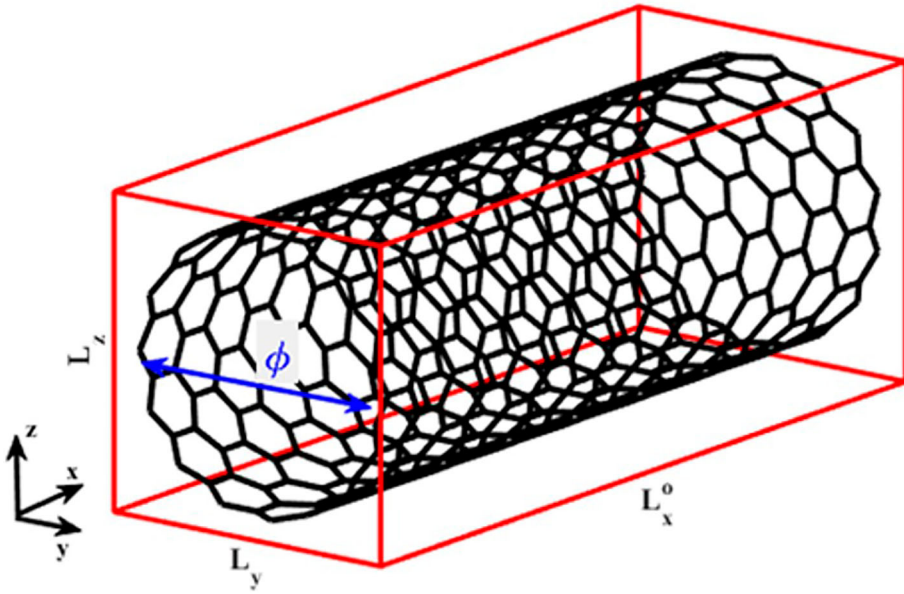


Figure 1. Schematic sample of SWCNT.

were considered. The diameters and initial lengths (L_x^0 , see Figure 1) of each nanotube are ~ 13.31 and 134.71 Å (zz), 13.58 and 147.8 Å (ch), and 13.56 and 136.31 Å (ar), respectively. Note that the length of the (9,11) nanotube is based on the translational vector's length to respect the chiral nanotube's periodicity. These geometric parameters provide an aspect ratio of ~ 10 for all directions, which was considered as a criterion for studying the chirality effects according to previous studies [38]. Other geometric parameters can be found elsewhere [39].

Figure 2 presents all the topological defect configurations. These defects were observed experimentally [40], and most of them represent a reconstruction of mono and divacancies. Figure 2a shows the nomenclature adopted for each defect: Stones-Wales (SW), being SW1 for the zz direction and SW2 for the ar and ch directions; the divacancy reconstructions 585, 555777, and 555567777; and the monovacancy reconstruction SV. The SW configuration is obtained by the rotation of a carbon-carbon bond at 90° . The divacancy reconstructions are formed when two atoms are removed from the perfect nanotube lattice followed by a rotation of one and two carbon-carbon bonds at 90° depending on the configuration.

According to ab-initio studies [21,22], the most stable and favourable defect configurations present a tilt concerning the nanotube axis in the ar direction, as shown in Figure 2b, while for the zz , they are parallel to the nanotube axis, as shown in Figure 2c. For completeness, as the ar and ch nanotubes present similar chiral angles, the same defect configurations used for the ar were

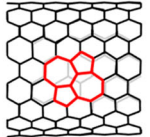
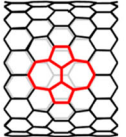
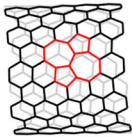
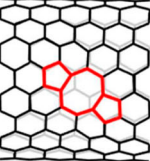
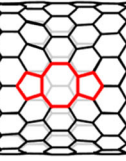
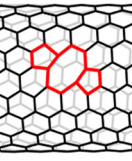
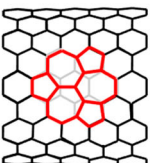
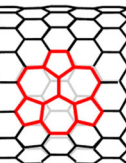
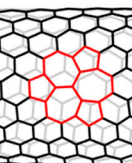
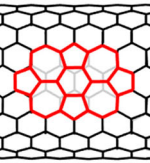
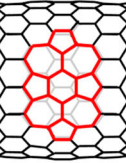
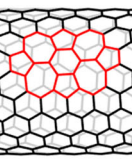
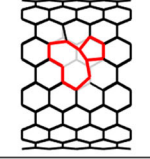
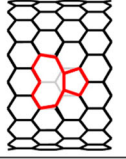
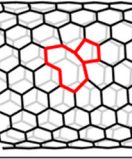
Defects	Directions		
	Armchair	Zigzag	Chiral
SW			
585			
555777			
555567777			
SV			
(a)	(b)	(c)	(d)

Figure 2. Topological defects embedded into the *ar*, *zz*, and *ch* SWCNTs.

considered for *ch* nanotubes, as shown in Figure 2d. Note that these representations correspond to a just small region of the nanotube where the defects were introduced.

Methodology

MD calculations were performed to investigate the mechanical response of defective SWCNTs under uniaxial tension loading, using the LAMMPS package [41]. The simulations were carried out based on the AIREBO potential, which has been widely employed to model carbon-based structures [42,43]. This potential consists of the sum of the second-generation reactive empirical bond order (REBO) potential, Lennard-Jones potential, and torsional interactions. We fully considered the second-generation reactive empirical bond order (REBO) potential and the Lennard-Jones potential contributions.

The AIREBO cut-off radii's role was discussed in the defect formation energy section, and the values were set as $R_1 = 1.97 \text{ \AA}$ and $R_2 = 2 \text{ \AA}$, following the values employed in other studies [42]. It is worth mentioning that there are limitations in the description of the fracture mechanisms using empirical potentials as the AIREBO [44]. For a deep understanding of the electronic structure basis on the fracture mechanisms, it is important to perform density functional theory calculations. However, as discussed by previous studies, modifying the cut-off function of the second-generation reactive empirical bond order (REBO) potential, AIREBO provides reasonable results for the fracture of SWCNTs [15,44]. This procedure makes possible analyses of a large number of atoms, which can still be prohibitively for a fully ab initio calculation.

Initially, for the tensile strain simulations, a conjugate gradient algorithm was employed to minimise the forces and energy. Then, we performed a pressure equilibration in NPT ensemble at 10 K and zero pressure. The temperature of 10 K and a time step of 0.5 fs were used in all MD simulations. The production runs were performed in the NVT ensemble, using the Nosé-Hoover thermostat. Uniaxial tensile tests were simulated by applying strain at a rate of 0.001 ps⁻¹ with imposing periodic boundary in the x-direction. Results for 300 K are presented in the Supplementary Information.

The SWCNTs' mechanical responses were presented in stress-strain curves and fracture strength and failure strain diagrams. The displacement obtains the strain, ΔL_x , divided by the original nanotube length L_x^0 (see Figure 1). The stress values were calculated by averaging the virial stress of each carbon atom. The thickness (t) is set as 3.4 Å. We properly calculated the stresses on the CNTs neglecting the simulation box as shown in Equation 1 [45],

$$\sigma_{\text{SWCNT}} = \frac{\sigma_{\text{sim_box}} L_y L_z}{\pi \phi t} \quad (1)$$

where the $\sigma_{\text{sim_box}}$ is the averaging virial stress obtained from the MD simulations, t is the thickness of 3.4 Å, ϕ is the diameters of the nanotubes, L_y and L_z are the lengths in y and z directions, respectively.

The formation energy was calculated in reference to the pristine SWCNT's enthalpy (PE) using the minimise command in LAMMPS. Then, the PE was used to obtain the defect formation energy ($E_{\text{def_form}}$) based on the expression [22]:

$$E_{\text{def_form}}(\text{Def}) = E_{\text{pot}}(\text{Def}) - E_{\text{pot}}(\text{Prist}) + N\mu_C \quad (2)$$

where $E_{\text{pot}}(\text{Def})$ and $E_{\text{pot}}(\text{Prist})$ are the potential energy of the defective and pristine CNTs, respectively. The term N is the number of removed atoms, and μ_C is the carbon chemical potential.

Results and discussion

Defect formation energies

As mentioned, it is still a challenge to synthesise CNTs without defect formation, and some defects are more energetically favourable than others, according to ab-initio studies. Thereby, the following results present the defect formation energy of SWCNTs obtained from MD simulations using the AIREBO potential.

Firstly, we investigated the influence of the AIREBO cut-off radii on the formation energies. Several studies [33,46–48] reported that the standard AIREBO potential with cut-off radii of $R1 = 1.7 \text{ \AA}$ and $R2 = 2 \text{ \AA}$ overestimates the forces calculations, leading to a non-physical failure mechanism. To avoid this problem, many authors have proposed to use cut-off radii $R1$ and $R2$ as 2 \AA . However, based on our study, the cut-off radii $R1 = R2 = 2 \text{ \AA}$ still provides inaccurate values for certain formation energies compared to ab-initio calculation. For instance, it was found formation energy of 30 eV for the *ar* SW2, using $R1 = R2 = 2 \text{ \AA}$. Therefore, we concluded that the maximum value for $R1$ must be 1.97 \AA .

Figure 3 presents the *ar*, *ch*, and *zz* SWCNTs' defect formation energy, considering all the configurations depicted in Figure 2. The defect formation

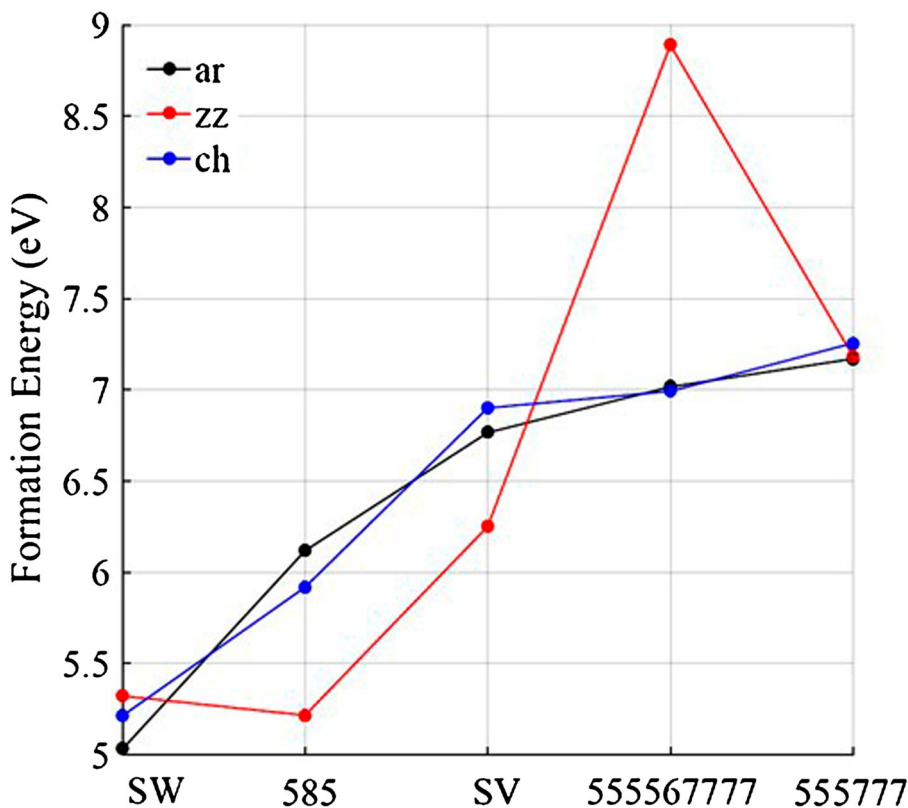


Figure 3. The defect formation energy of the *ar* (black curve), *ch* (blue curve), and *zz*.

energy curves are similar in the *ar* and *ch* directions. For both, the SW is the most stable configuration compared to the other defects, followed by the 585, SV, 555567777, and 555777. For the *zz*, 585 is the most stable configuration, followed by the SW, SV, 555777, and 555567777.

Our results agree qualitatively with the ones presented by the ab-initio studies. According to Amorim et al. [21], along the *ar* direction, the most stable and favourable defect is the SW followed by the 585, 555777, and SV, the same is for the *zz* direction, the most favourable is the SW followed by the 585, 555777, and SV. Based on the Padilha et al. [22] study, along the *ar* direction, the 585 defect is the most favourable compared to the 555567777 and 555777, and the 555567777 is the most favourable than the 555777. The trend of the curves shown in Figure 3 along the *ar* and *zz* directions agree with the sequence described by Amorim et al. [21], except for the *ar* SV and the *zz* 585, while in the *ar*, the curve agrees well with the sequence described by Padilha et al. [22]. Despite this quantitative discrepancy reported here, simulations based on empirical potentials qualitatively follow ab-initio calculations on the prediction of the defect formation energies.

Mechanical response of defective SWCNTs

The following results show the defect effects on SWCNTs' mechanical response in the *zz*, *ch*, and *ar* directions. Each nanotube has a single defect embedded into its wall.

The stress–strain curves in the three directions show a significant reduction in the fracture stress and failure strain than the pristine SWCNTs, as depicted in Figure 4. The defective *ch* and *ar* SWCNTs present fracture stress and strain in a range of 80–98 GPa and 12%–17% (Pristine: 109.7–111.9 GPa and 24%–26%), respectively, while for the defective *zz* SWCNT, the fracture stress is in a range of 70–91 GPa and the failure strain of 8%–14% (Pristine: 95.4 GPa and 17%). In general, the defective *zz* SWCNTs are weak and less ductile compared to the defective *ar* and *ch* SWCNTs.

The stress–strain curves remain similar in the *ar* and *ch* directions until strains of ~11%, showing a minor effect of the defects' configurations, whereas, in the *zz* direction, the effect appears at strains of ~ 8% (See Figure 4). Comparing the curves in the three directions, they do not follow the same trend, even for the *ar* and *ch* directions that have a similar chiral angle. This behaviour confirms the chirality and the defect' configuration effects on the mechanical response of defective SWCNTs, which became more significant at strains >8%.

The SW defect is one of the most common configurations formed during the synthesis of carbon structures. According to ab-initio studies and our results (for the *ar* and *ch*), this defect is the most favourable to form in the CNT structure than other defects. Such defect reduces the strength by 13.5% in the *ar*

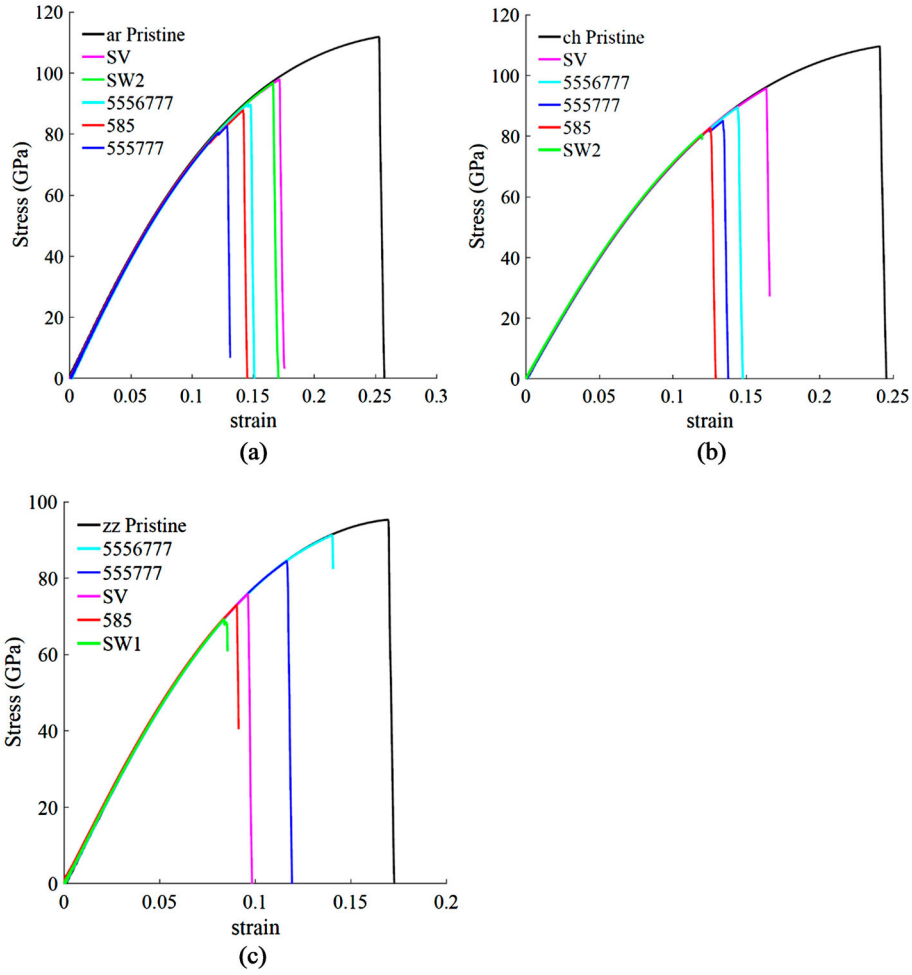


Figure 4. Stress-strain curves of defective SWCNTs in the (a) *ar*, (b) *ch*, (c) *zz* directions.

direction, while in the *ch* and *zz* directions, the strength is reduced by 26.5% and 27.4%, respectively. The fracture stress and strain of the *ar*, *ch*, and *zz* SWCNTs are 96.8, 80.6, 69.3 GPa, and 0.17, 0.12, and 0.08, respectively. Using molecular dynamics, Belytschko et al. [33] simulated a (12,12) SWCNT with the SW defect. They obtained fracture stress and strain of 97.5 GPa and 14.3%, respectively. Our results along the *ar* direction are in good agreement with these values. Tserpes et al. [49], using the finite element method and modified Morse interatomic potential, calculated the fracture stress and strain of the (12,12), (16,8), and (20,0) SWCNTs with the SW defect. They found that the failure stress and strain are 100, 96.85, and 97.68 GPa and 11.96%, 12.1%, and 15.75%, respectively. These values present a reasonable agreement with current values for the *ar* and *ch* defective nanotubes, except for the defective *zz* SWCNTs. The discrepancy observed here could be assigned to the different methodologies and potential energy considered at each study.

The stress–strain curves of the SV defect showed that the monovacancy is stronger and more ductile compared to the other defects in the *ar* and *ch* directions, while along the *zz* direction, SV is weaker compared to the 555777 and 555567777 defects. The *ar* SWCNTs with the SV and SW2 defects showed a similar reduction in strength, while the strength is less affected by SV's presence than the SW in the *ch* and *zz* directions. The SV reduces the strength by 12.5%, 13.4%, and 20.49% in the *ar*, *ch*, and *zz* directions. Sammalkorpi et al. [26], using MD simulations and continuum theory, found that the reconstructed defects, such as single, double, and triple vacancies, can decrease the tensile strength by 10–15% for the *ar* nanotubes and 5–10% for the *zz* nanotubes. Zhang et al. [15] reported a reduction in nanotubes' fracture strength with monovacancy and divacancy by 20%–33%. For the *zz* nanotubes with SV defect, they found a fracture strength reduction of ~26%. These results are in concordance with the reductions reported in this study, except for the *zz* nanotube. It is worth mentioning that, contrary to damage that the SV defects can cause to SWCNT's mechanical response, they have been used to increasing the friction and shear strength between CNT walls [48,50].

Another common defect formed during the synthesis of carbon structures is the reconstructions of the divacancy commonly known as 585, 555777, and 555567777. Several studies have considered these configurations to investigate their effects on carbon structures' electronic properties [51–55]. However, no previous study has investigated their impact on SWCNTs' mechanical response under tension in the three directions, as well as and their effects compared to the SV and SW defects to the best of our knowledge.

The stress–strain curves shown in Figure 4 confirm that the 555567777 is the most strong and ductile compared to the 585 and 555777 in the three directions and compared to all defects in the *ar* direction. The same behaviour has been reported [56] for the *zz* graphene, which corresponds to the *ar* 555567777 SWCNT in this study. The fracture stress and strain of the 555567777 SWCNT are around 89.94 GPa and 0.15 (*ar*), 89.61 GPa and 0.15 (*ch*), and 91.32 GPa and 0.14 (*zz*), respectively.

According to ab-initio studies and our results, the 585 configuration presents low defect formation energy. Its presence on the nanotube shows a substantial reduction in the fracture stress of 21.5%, 24.6%, and 23.4% in the *ar*, *ch*, and *zz* directions, respectively. Zhang et al. [15] found a larger reduction of the fracture stress compared with our results, with values of ~30% and 26% for the (5,5) and (10,0) SWCNTs, respectively. Comparing the divacancy reconstructions with the other defects, the configuration 555567777 has less significant effect on the tensile strength properties of SWCNTs in all directions.

Therefore, we conclude that the defective *zz* SWCNTs are weak and less ductile than the defective *ar* and *ch* SWCNTs, like in the pristine cases. Comparing the stress–strain curves, they do not follow the same trend, even for *ar* and *ch* directions with a similar chiral angle. The stress–strain curves are notably

dependent on the chirality, where the effect of the defect's configuration becomes more significant at strains over 8%. The 555567777 is the strongest configuration compared to the other defects in the zz direction. The two most favourable and stable configurations, SW and 585, have a high impact on the mechanical response of SWCNTs, with strength reduction over 14%, 21%, and 23% in the ar , ch , and zz directions, respectively. Note that the described mechanical behaviour is for 10 K, and at higher temperatures, this behaviour can change and have a higher impact on the mechanical response of the SWCNTs. The stress–strain curves for 300 K are presented in the Supplementary Information.

Mechanical response of SWCNTs with multiple topological defects

In this section, the effect of multiple topological defects on the ar and zz SWCNTs' mechanical response was investigated. The SW and 585 defects were chosen due to present the lowest formation energies. Figure 5 shows an illustration (side view) of the SWCNTs with the combination of these defects in three different configurations called CNT_1, CNT_2, and CNT_3. In the configuration CNT_1, there are five 585 defects spaced by a similar distance along the nanotube length. Note that as it was imposed periodic boundary condition in the x -direction, the last defects in the extremities have a larger distance between them than the ones in the nanotubes' core. In the CNT_2 and CNT_3 configurations, there are five 585 defects spaced by a similar distance, and one SW2 (See Figure 5). The same arrangements are considered in the zz direction, but with the defects' orientations presented in Figure 2c.

Figure 6 shows the fracture strength and failure strain curves of the three proposed configurations in the ar and zz directions. For both directions, there is no significant reduction or enhancement of strength and strain by combining the 585 and SW defects. On the other hand, the configurations' fracture patterns showed an interesting behaviour when the SW was placed at different

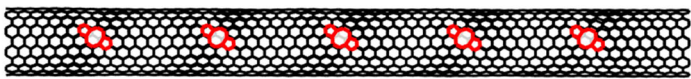
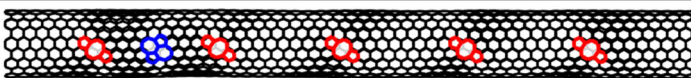
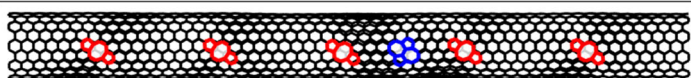
Configurations	ar SWCNT
CNT_1	
CNT_2	
CNT_3	

Figure 5. Side view of schematic samples of ar SWCNTs with the combination of the 585 and SW2 defects.

positions. To illustrate this behaviour, Figure 7 shows the potential energy (PE) and the strain energy (SE) distributions of the ar CNT_1 during the stretching process.

Figure 7a shows the PE distribution for strain equal to zero. As expected, higher values were found around the defects. The SE distributions at strains of 0.1, 0.1075, and 0.117 were presented in Figure 7b–d. The SE at $\varepsilon = 0.1075$ is almost twice the SE at $\varepsilon = 0.1$ with a value of ~ 1.2 eV. The system started to fail at $\varepsilon = 0.117$ with a SE level > 2.5 eV (See Figure 7d). To illustrate the fracture pattern, Figure 7e shows a zoom-in picture of the defect where the failure happened. For $\varepsilon = 0.1$, two carbon–carbon atoms at each side of the defect present higher SE values (> 0.6 eV). The same bonds remained with higher SE values until $\varepsilon = 0.1075$, with the bond on the top side exhibiting higher strain energies. Consequently, the fracture happened firstly on this bond, which was shared by a hexagon-octagon (See Figure 7e). After this point, the failure propagated through the nanotube's diameter.

The same analyses were performed for the CNT_2. Interestingly, introducing the SW2 close to the first 585 on the left side, the fracture moved closer to the SW2 and started on the first 585, as shown in Figure 8b and c. Contrary to the previous case, this configuration failed at $\varepsilon = 0.1125$ with a higher SE level over 3.0 eV. To illustrate the fracture pattern, Figure 8c–d show a zoom-in picture of the defects numbered as 1 and 2. Like in the previous case, the fracture happened on the hexagon-octagon bond (See Figure 8c), showing that the presence of the SW had no significant influence on the SE level but a significant influence on the fracture position. The SW2 SE level remained practically the same for all strain levels, as shown in Figure 8d.

Performing the same analyses for the CNT_3 (see Figure 5), we observed that the fracture moved closer to the SW2 and started on the fourth 585 (right side).

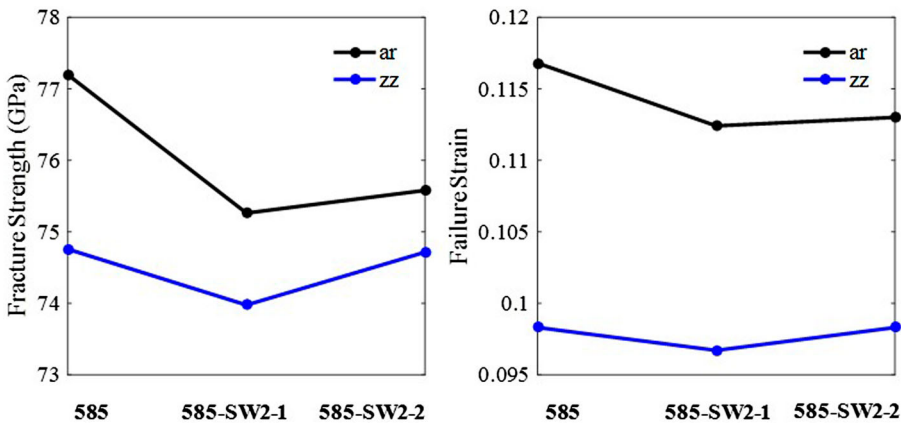


Figure 6. Fracture strength and failure strain of the CNT_1, CNT_2, and CNT_3 configurations in the ar and zz directions.

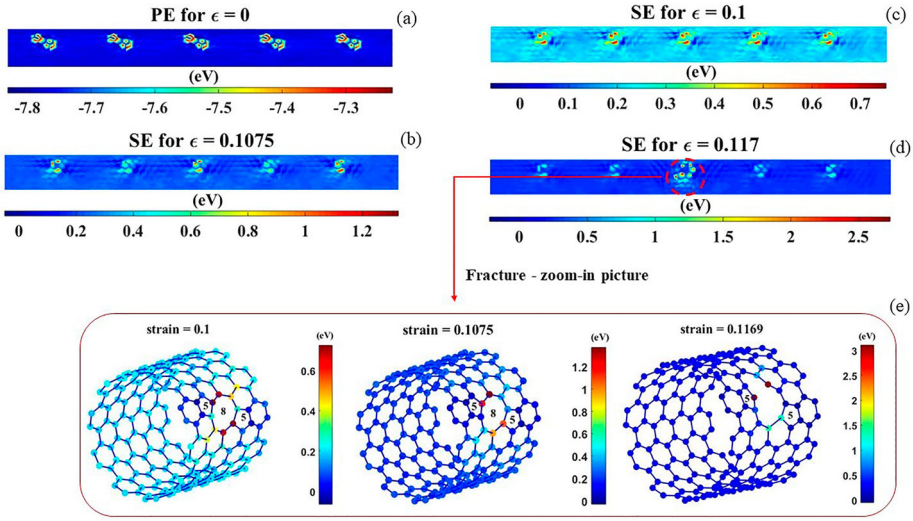


Figure 7. Side view of the *ar* CNT_1: (a) potential energy (PE), (b)-(d) strain energy (SE) for different strain levels (ϵ), and (e) zoom-in picture of the defect where the fracture happened.

This behaviour is similar to the CNT_2, and the only difference is the fracture location. From the combination of the 585 and SW defects, the 585 showed more prone to concentrate higher strain energy values compared to the SW, which remained unchanged during the stretching process. In both CNT_2 and CNT_3, the fracture happened in the region close to the SW defect, indicating a possibility of manipulating the fracture patterns using defects.

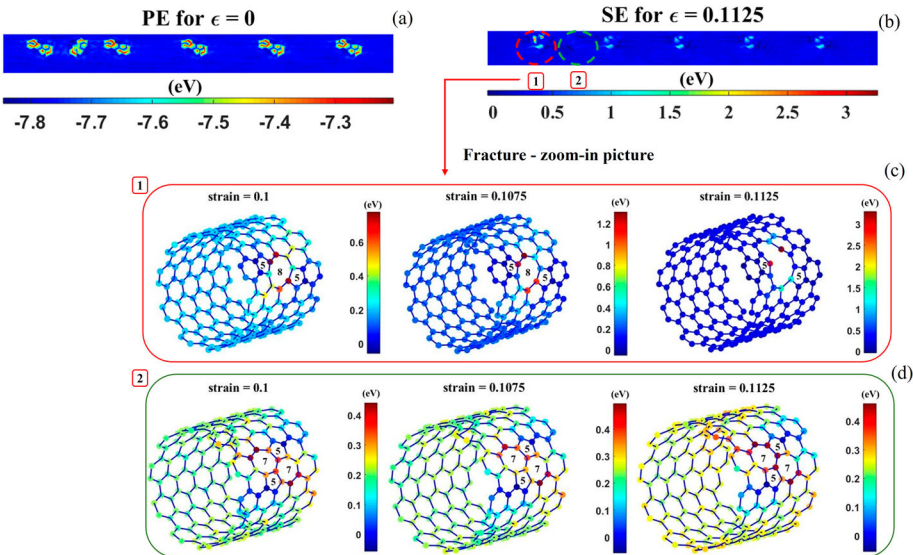


Figure 8. Side view of the *ar* CNT_2: (a) potential energy (PE), (b) strain energy (SE), and (c)-(d) zoom-in picture of the 585 and SW2 defects.

For completeness, the same analyses were carried out considering the configurations under compression loading (See supplementary information). The results reveal that the buckling happened in the same region where the nanotubes failed when they were under tension loading, indicating that the fracture area is more affected by the defect configurations and concentration than the loading condition. Furthermore, we repeated the same procedure, but instead of adding the SW defect, another 585 was added to the system. Under tension loading, the fracture pattern showed do not follow the same rule as in the previous cases, exhibiting a complex dependence on the defect shape and orientation.

Conclusions

We investigated the effects of chirality and single and multiple defects on the mechanical response of SWCNTs using MD simulations. Discussion related to the defect formation energy using the AIREBO potential was also addressed.

The results reveal that the AIREBO potential with modified cut-off radii can qualitatively predict the more stable defects. The defective *zz* SWCNTs are weak and less ductile than the defective *ar* and *ch* SWCNTs. Comparing the stress–strain curves of defective SWCNTs in the three directions, they do not follow the same trend, even for *ar* and *ch* directions with a similar chiral angle.

The stress–strain curves behaviour of defective SWCNTs is notably dependent on the chirality, which becomes more significant at strains over 8%. The 555567777 configuration is the most strong and ductile compared to the other reconstructed divacancies in the three directions. The two most favourable and stable configurations, SW and 585, have a high impact on the mechanical response of SWCNTs, with strength reduction over 14%, 21%, and 23% in the *ar*, *ch*, and *zz* directions, respectively.

No significant reduction or enhancement of strength and strain was observed from the combination of the SW and 585 defects. The 585 defects showed more prone to concentrate high values of strain energy compared to the SW. The simulations also reveal that the fracture area is more affected by the defect configuration and concentration than the loading mode. We hope the findings of this study help to open a new perspective on how to control the fracture pattern using defects, which could significantly contribute to the designing of innovative nanostructures with tailored properties.

Acknowledgments

We gratefully acknowledge support of the RCGI – Research Centre for Gas Innovation, hosted by the University of São Paulo (USP) and sponsored by FAPESP – São Paulo Research Foundation (2014/50279-4, 2020/15230-5, and project number 2020/01558-9)

and Shell Brasil, and the strategic importance of the support given by ANP (Brazil's National Oil, Natural Gas and Biofuels Agency) through the R&D levy regulation. The authors also acknowledge National Council for Scientific and Technological Development (CNPq) through grant 307064/2019-0 for financial support. The computational time for the calculations was provided by High-Performance Computing facilities at the University of de São Paulo (USP).

Disclosure statement

No potential conflict of interest was reported by the author(s).

Funding

We gratefully acknowledge support of the RCGI – Research Centre for Gas Innovation, hosted by the University of São Paulo (USP) and sponsored by FAPESP – São Paulo Research Foundation (2014/50279-4, 2020/15230-5, and project number 2020/01558-9) and Shell Brasil, and the strategic importance of the support given by ANP (Brazil's National Oil, Natural Gas and Biofuels Agency) through the R&D levy regulation. The authors also acknowledge National Council for Scientific and Technological Development (CNPq) through grant 307064/2019-0 for financial support. The computational time for the calculations was provided by High-Performance Computing facilities at the University of de São Paulo (USP).

Data availability

The data is available under direct request to the authors.

Author contributions

Conceptualisation, methodology, MD implementation, investigation, numerical results, writing original draft, editing: **DAD**. Conceptualisation, methodology and data analysis, supervision, funding author 1, and manuscript editing: **CRM**. All authors have read and agreed to the manuscript's published version.

ORCID

Daniela A. Damasceno  <http://orcid.org/0000-0002-7660-982X>

Caetano R. Miranda  <http://orcid.org/0000-0002-8008-4907>

References

- [1] S. Iijima and T. Ichihashi, *Single-shell carbon nanotubes of 1-nm diameter*. Nature 363 (1993), pp. 603–605. doi:[10.1038/363603a0](https://doi.org/10.1038/363603a0).
- [2] P. Bernardo, E. Drioli and G. Golemme, *Membrane gas separation: A review/state of the art*. Ind. Eng. Chem. Res 48 (2009), pp. 4638–4663. doi:[10.1021/ie8019032](https://doi.org/10.1021/ie8019032).

- [3] J.K. Holt, *Fast mass transport through sub-2-nanometer carbon nanotubes*. Science (80-.) 312 (2006), pp. 1034–1037. doi:[10.1126/science.1126298](https://doi.org/10.1126/science.1126298).
- [4] C. Lee, X. Wei, J.W. Kysar and J. Hone, *Measurement of the elastic properties and intrinsic strength of monolayer graphene*. Science (80-.) 321 (2008), pp. 385–388. doi:[10.1126/science.1157996](https://doi.org/10.1126/science.1157996).
- [5] R. Zhang, Q. Wen, W. Qian, D.S. Su, Q. Zhang and F. Wei, *Superstrong ultralong carbon nanotubes for mechanical energy storage*. Adv. Mater 23 (2011), pp. 3387–3391. doi:[10.1002/adma.201100344](https://doi.org/10.1002/adma.201100344).
- [6] M.K. Purkait and R. Singh, *Membrane Technology in Separation Science*, CRC Press, Boca Raton, 2018. doi:[10.1201/9781315229263](https://doi.org/10.1201/9781315229263).
- [7] J. Mittal and K.L. Lin, *Carbon nanotube-based interconnections*. J. Mater. Sci. 52 (2017), pp. 643–662. doi:[10.1007/s10853-016-0416-4](https://doi.org/10.1007/s10853-016-0416-4).
- [8] A. Takakura, K. Beppu, T. Nishihara, A. Fukui, T. Kozeki, T. Namazu, Y. Miyauchi and K. Itami, *Strength of carbon nanotubes depends on their chemical structures*. Nat. Commun 10 (2019), pp. 1–7. doi:[10.1038/s41467-019-10959-7](https://doi.org/10.1038/s41467-019-10959-7).
- [9] C. Chang, I. Hsu, M. Aykol, W. Hung, C. Chen and S.B. Cronin, *A new lower limit for the ultimate breaking strain of carbon nanotubes*. ACS Nano 4 (2010), pp. 5095–5100. doi:[10.1021/nn100946q](https://doi.org/10.1021/nn100946q).
- [10] R.S. Ruoff, D. Qian and W.K. Liu, *Mechanical properties of carbon nanotubes: theoretical predictions and experimental measurements*. Comptes Rendus Phys 4 (2003), pp. 993–1008. doi:[10.1016/j.crhy.2003.08.001](https://doi.org/10.1016/j.crhy.2003.08.001).
- [11] M. Yu, *Strength and breaking mechanism of multiwalled carbon nanotubes under tensile load*. Science (80-.) 287 (2000), pp. 637–640. doi:[10.1126/science.287.5453.637](https://doi.org/10.1126/science.287.5453.637).
- [12] K.M. Liew, Y. Jianwei and L.-W. Zhang, *Mechanical Behaviors of Carbon Nanotubes: Theoretical and Numerical Approaches*, Elsevier: Amsterdam, Netherlands, 2017.
- [13] H. Yazdani, K. Hatami and M. Eftekhari, *Mechanical properties of single-walled carbon nanotubes: a comprehensive molecular dynamics study*. Mater. Res. Express. 4 (2017), pp. 055015. doi:[10.1088/2053-1591/aa7003](https://doi.org/10.1088/2053-1591/aa7003).
- [14] L. Zhu, J. Wang and F. Ding, *The great reduction of a carbon nanotube's mechanical performance by a few topological defects*. ACS Nano 10 (2016), pp. 6410–6415. doi:[10.1021/acsnano.6b03231](https://doi.org/10.1021/acsnano.6b03231).
- [15] S. Zhang, S.L. Mielke, R. Khare, D. Troya, R.S. Ruoff, G.C. Schatz and T. Belytschko, *Mechanics of defects in carbon nanotubes: Atomistic and multiscale simulations*. Phys. Rev. B 71 (2005), pp. 115403. doi:[10.1103/PhysRevB.71.115403](https://doi.org/10.1103/PhysRevB.71.115403).
- [16] F.A.L. de Souza, R.G. Amorim, J. Prasongkit, W.L. Scopel, R.H. Scheicher and A.R. Rocha, *Topological line defects in graphene for applications in gas sensing*. Carbon N. Y. 129 (2018), pp. 803–808. doi:[10.1016/j.carbon.2017.11.029](https://doi.org/10.1016/j.carbon.2017.11.029).
- [17] G.P. Tang, J.C. Zhou, Z.H. Zhang, X.Q. Deng and Z.Q. Fan, *A theoretical investigation on the possible improvement of spin-filter effects by an electric field for a zigzag graphene nanoribbon with a line defect*. Carbon N. Y. 60 (2013), pp. 94–101. doi:[10.1016/j.carbon.2013.04.002](https://doi.org/10.1016/j.carbon.2013.04.002).
- [18] M. Terrones, P.M. Ajayan, F. Banhart, X. Blase, D.L. Carroll, J.C. Charlier, R. Czerw, B. Foley, N. Grobert, R. Kamalakaran, P. Kohler-Redlich, M. Rühle, T. Seeger and H. Terrones, *N-doping and coalescence of carbon nanotubes: Synthesis and electronic properties*. Appl. Phys. A Mater. Sci. Process. 74 (2002), pp. 355–361. doi:[10.1007/s003390201278](https://doi.org/10.1007/s003390201278).
- [19] B. Kumaneck and D. Janas, *Thermal conductivity of carbon nanotube networks: A review*. J. Mater. Sci 54 (2019), pp. 7397–7427. doi:[10.1007/s10853-019-03368-0](https://doi.org/10.1007/s10853-019-03368-0).

- [20] S.L. Lair, W.C. Herndon and L.E. Murr, *Energetic trends of single-walled carbon nanotube ab initio calculations*. J. Mater. Sci 42 (2007), pp. 1819–1827. doi:[10.1007/s10853-006-0815-z](https://doi.org/10.1007/s10853-006-0815-z).
- [21] R.G. Amorim, A. Fazzio, A. Antonelli, F.D. Novaes and A.J.R. da Silva, *Divacancies in graphene and carbon nanotubes*. Nano Lett. 7 (2007), pp. 2459–2462. doi:[10.1021/nl071217v](https://doi.org/10.1021/nl071217v).
- [22] J.E. Padilha, R.G. Amorim, A.R. Rocha, A.J.R. da Silva and A. Fazzio, *Energetics and stability of vacancies in carbon nanotubes*. Solid State Commun. 151 (2011), pp. 482–486. doi:[10.1016/j.ssc.2010.12.031](https://doi.org/10.1016/j.ssc.2010.12.031).
- [23] H. Mori, Y. Hirai, S. Ogata, S. Akita and Y. Nakayama, *Chirality dependence of mechanical properties of single-walled carbon nanotubes under axial tensile strain*. Jpn. J. Appl. Phys 44 (2005), pp. L1307–L1309. doi:[10.1143/JJAP.44.L1307](https://doi.org/10.1143/JJAP.44.L1307).
- [24] T. Ragab and C. Basaran, *A framework for stress computation in single-walled carbon nanotubes under uniaxial tension*. Comput. Mater. Sci 46 (2009), pp. 1135–1143. doi:[10.1016/j.commatsci.2009.05.022](https://doi.org/10.1016/j.commatsci.2009.05.022).
- [25] B. WenXing, Z. ChangChun and C. WanZhao, *Simulation of Young's modulus of single-walled carbon nanotubes by molecular dynamics*. Phys. B Condens. Matter 352 (2004), pp. 156–163. doi:[10.1016/j.physb.2004.07.005](https://doi.org/10.1016/j.physb.2004.07.005).
- [26] M. Sammalkorpi, A. Krashenninnikov, A. Kuronen, K. Nordlund and K. Kaski, *Mechanical properties of carbon nanotubes with vacancies and related defects*. Phys. Rev. B 70 (2004), pp. 245416. doi:[10.1103/PhysRevB.70.245416](https://doi.org/10.1103/PhysRevB.70.245416).
- [27] J.Y. Hsieh, J.M. Lu, M.Y. Huang and C.C. Hwang, *Theoretical variations in the Young's modulus of single-walled carbon nanotubes with tube radius and temperature: A molecular dynamics study*. Nanotechnology 17 (2006), pp. 3920–3924. doi:[10.1088/0957-4484/17/15/051](https://doi.org/10.1088/0957-4484/17/15/051).
- [28] C.C. Hwang, Y.C. Wang, Q.Y. Kuo and J.M. Lu, *Molecular dynamics study of multi-walled carbon nanotubes under uniaxial loading*. Phys. E Low-Dimensional Syst. Nanostructure 42 (2010), pp. 775–778. doi:[10.1016/j.physe.2009.10.064](https://doi.org/10.1016/j.physe.2009.10.064).
- [29] J.M. Lu, C.C. Hwang, Q.Y. Kuo and Y.C. Wang, *Mechanical buckling of multi-walled carbon nanotubes: The effects of slenderness ratio*. Phys. E Low-Dimensional Syst. Nanostructure 40 (2008), pp. 1305–1308. doi:[10.1016/j.physe.2007.08.120](https://doi.org/10.1016/j.physe.2007.08.120).
- [30] G. Cao and X. Chen, *The effects of chirality and boundary conditions on the mechanical properties of single-walled carbon nanotubes*. Int. J. Solids Struct 44 (2007), pp. 5447–5465. doi:[10.1016/j.ijsolstr.2007.01.005](https://doi.org/10.1016/j.ijsolstr.2007.01.005).
- [31] M. Meo and M. Rossi, *Tensile failure prediction of single wall carbon nanotube*. Eng. Fract. Mech 73 (2006), pp. 2589–2599. doi:[10.1016/j.engfracmech.2006.05.005](https://doi.org/10.1016/j.engfracmech.2006.05.005).
- [32] A.F. Ávila and G.S.R. Lacerda, *Molecular mechanics applied to single-walled carbon nanotubes*. Mater. Res 11 (2008), pp. 325–333. doi:[10.1590/S1516-14392008000300016](https://doi.org/10.1590/S1516-14392008000300016).
- [33] T. Belytschko, S.P. Xiao, G.C. Schatz and R.S. Ruoff, *Atomistic simulations of nanotube fracture*. Phys. Rev. B – Condens. Matter Mater. Phys 65 (2002), pp. 2354301–2354308. doi:[10.1103/PhysRevB.65.235430](https://doi.org/10.1103/PhysRevB.65.235430).
- [34] P.S. Rao, S. Anandatheertha, G.N. Naik and S. Gopalakrishnan, *Estimation of mechanical properties of single wall carbon nanotubes using molecular mechanics approach*. Sadhana 40 (2015), pp. 1301–1311. doi:[10.1007/s12046-015-0367-5](https://doi.org/10.1007/s12046-015-0367-5).
- [35] B. Liu, H. Jiang, Y. Huang, S. Qu, M.F. Yu and K.C. Hwang, *Atomic-scale finite element method in multiscale computation with applications to carbon nanotubes*. Phys. Rev. B 72 (2005), pp. 035435. doi:[10.1103/PhysRevB.72.035435](https://doi.org/10.1103/PhysRevB.72.035435).
- [36] S.J. Stuart, A.B. Tutein and J.A. Harrison, *A reactive potential for hydrocarbons with intermolecular interactions*. J. Chem. Phys 112 (2000), pp. 6472–6486. doi:[10.1063/1.481208](https://doi.org/10.1063/1.481208).

- [37] D.W. Brenner, O.A. Shenderova, J.A. Harrison, S.J. Stuart, Boris Ni and Susan B Sinnott, *A second-generation reactive empirical bond order (REBO) potential energy expression for hydrocarbons*. Mater. Sci 14 (2002), pp. 783–802. doi:[10.1088/0953-8984/14/4/312](https://doi.org/10.1088/0953-8984/14/4/312).
- [38] H. Yazdani, K. Hatami and M. Eftekhari, *Mechanical properties of single-walled carbon nanotubes: a comprehensive molecular dynamics study*. Mater. Res. Express 4 (2017), pp. 055015. doi:[10.1088/2053-1591/aa7003](https://doi.org/10.1088/2053-1591/aa7003).
- [39] M.S. Dresselhaus, G. Dresselhaus and R. Saito, *Physics of carbon nanotubes*. Carbon N. Y. 33 (1995), pp. 883–891. doi:[10.1016/0008-6223\(95\)00017-8](https://doi.org/10.1016/0008-6223(95)00017-8).
- [40] J. Kotakoski, A.V. Krasheninnikov, U. Kaiser and J.C. Meyer, *From point defects in graphene to two-dimensional amorphous carbon*. Phys. Rev. Lett 106 (2011), pp. 1–4. doi:[10.1103/PhysRevLett.106.105505](https://doi.org/10.1103/PhysRevLett.106.105505).
- [41] S. Plimpton, *Fast parallel algorithms for short-range molecular dynamics*. J. Comput. Phys 117 (1995), pp. 1–19. doi:[10.1006/jcph.1995.1039](https://doi.org/10.1006/jcph.1995.1039).
- [42] A.R. Alian and S.A. Meguid, *A critical study of the parameters governing molecular dynamics simulations of nanostructured materials*. Comput. Mater. Sci 153 (2018), pp. 183–199. doi:[10.1016/j.commatsci.2018.06.028](https://doi.org/10.1016/j.commatsci.2018.06.028).
- [43] Y. Liu and X. Chen, *Mechanical properties of nanoporous graphene membrane*. J. Appl. Phys 115 (2014), pp. 034303. doi:[10.1063/1.4862312](https://doi.org/10.1063/1.4862312).
- [44] D. Troya, S.L. Mielke and G.C. Schatz, *Carbon nanotube fracture – Differences between quantum mechanical mechanisms and those of empirical potentials*. Chem. Phys. Lett 382 (2003), pp. 133–141. doi:[10.1016/j.cplett.2003.10.068](https://doi.org/10.1016/j.cplett.2003.10.068).
- [45] S.-H. Tzeng and J.-L. Tsai, *Characterizing the mechanical properties of graphene and single walled carbon nanotubes*. J. Mech 27 (2011), pp. 461–467. doi:[10.1017/jmech.2011.49](https://doi.org/10.1017/jmech.2011.49).
- [46] J. Leyssale and G.L. Vignoles, *A large-scale molecular dynamics study of the divacancy defect in graphene*. J. Phys. Chem. C 118 (2014), pp. 8200–8216. doi:[10.1021/jp501028n](https://doi.org/10.1021/jp501028n).
- [47] S.T. Skowron, I.V. Lebedeva, A.M. Popov and E. Bichoutskaia, *Energetics of atomic scale structure changes in graphene*. Chem. Soc. Rev 44 (2015), pp. 3143–3176. doi:[10.1039/c4cs00499j](https://doi.org/10.1039/c4cs00499j).
- [48] A.V. Krasheninnikov and K. Nordlund, *Ion and electron irradiation-induced effects in nanostructured materials*. J. Appl. Phys 107 (2010), pp. 071301. doi:[10.1063/1.3318261](https://doi.org/10.1063/1.3318261).
- [49] K.I. Tserpes and P. Papanikos, *The effect of Stone – Wales defect on the tensile behavior and fracture of single-walled carbon nanotubes*. Compos. Struct 79 (2007), pp. 581–589. doi:[10.1016/j.compstruct.2006.02.020](https://doi.org/10.1016/j.compstruct.2006.02.020).
- [50] M. Huhtala, A.V. Krasheninnikov, J. Aittoniemi, S.J. Stuart, K. Nordlund and K. Kaski, *Improved mechanical load transfer between shells of multiwalled carbon nanotubes*. Phys. Rev. B – Condens. Matter Mater. Phys 70 (2004), pp. 1–8. doi:[10.1103/PhysRevB.70.045404](https://doi.org/10.1103/PhysRevB.70.045404).
- [51] C. Gómez-Navarro, P.J. De Pablo, J. Gómez-Herrero, B. Biel, F.J. Garcia-Vidal, A. Rubio and F. Flores, *Tuning the conductance of single-walled carbon nanotubes by ion irradiation in the Anderson localization regime*. Nat. Mater 4 (2005), pp. 534–539. doi:[10.1038/nmat1414](https://doi.org/10.1038/nmat1414).
- [52] C.G. Rocha, T.G. Dargam and A. Latgé, *Electronic states in zigzag carbon nanotube quantum dots*. Phys. Rev. B – Condens. Matter Mater. Phys 65 (2002), pp. 1–7. doi:[10.1103/PhysRevB.65.165431](https://doi.org/10.1103/PhysRevB.65.165431).
- [53] L. Vicarelli, S.J. Heerema, C. Dekker and H.W. Zandbergen, *Controlling defects in graphene for optimizing the electrical properties of graphene nanodevices*. ACS Nano 9 (2015), pp. 3428–3435. doi:[10.1021/acs.nano.5b01762](https://doi.org/10.1021/acs.nano.5b01762).

- [54] J. Stehr, I. Buyanova and W. Chen, *Defects in Advanced Electronic Materials and Novel Low Dimensional Structures*, 1st ed., Woodhead Publishing: Duxford, UK, 2018.
- [55] A. Kirch, J.M. de Almeida and C.R. Miranda, *Multilevel molecular modeling approach for a rational design of ionic current sensors for nanofluidics*. J. Chem. Theory Comput 14 (2018), pp. 3113–3120. doi:[10.1021/acs.jctc.8b00073](https://doi.org/10.1021/acs.jctc.8b00073).
- [56] D.A. Damasceno, R.K.N.D. Rajapakse, E. Mesquita and R. Pavanello, *Atomistic simulation of tensile strength properties of graphene with complex vacancy and topological defects*. Acta Mech. (2020), pp. 3387–3404. doi:[10.1007/s00707-020-02715-6](https://doi.org/10.1007/s00707-020-02715-6).